1

Angle Sensor for Measurement of Surface Slope and Tilt Motion

1.1 Introduction

Angle is one of the most fundamental quantities for precision nanometrology. Angle sensors based on the principle of autocollimation, which are conventionally called autocollimators, can accurately measure small tilt angles of a light-reflecting flat surface [1]. Autocollimators have a long history of being used in metrology laboratories for calibration of angle standards, such as polygons, rotary index tables and angle gage blocks. They are also traditionally used in machine shops for surface profile measurements of straightedges, machine tool guideways, precision surface plates, as well as for measurement of tilt error motions of translational stages [2].

In a conventional photoelectric autocollimator, the light rays from a filament lamp are collimated to a parallel light beam with a large beam size, on the order of 30 to 50 mm in diameter [3]. The beam is then projected onto a flat target mirror mounted on the specimen surface. The deviation of the reflected beam with respect to the axis of the incident beam is detected by the autocollimation unit, which is composed of an objective lens and a light position detector placed at the focal plane of the objective lens. Autocollimators using CCD image sensors with image processing can achieve a resolution of up to 0.01 arcsec through employing an objective lens with a long focal length, typically on the order of 300 to 400 mm [3–6]. The large dynamic range of the CCD image sensor also makes the autocollimator have a dynamic range of 60 to 80 dB. However, the requirement of a large target mirror makes it difficult to measure soft specimens such as diamond turned optical surfaces, or thin specimens such as silicon wafers because the target mirror may damage the specimen. The large diameter of the light beam from the filament lamp also limits the lateral resolution for detecting the local slope of a surface. The low bandwidth and large dimension are other disadvantages of conventional autocollimators for the measurement of dynamic tilt error motions of a stage.

This chapter presents angle sensors using different types of photodiodes instead of CCD image sensors for improving the measurement speed and reduction of the sensor size.

1.2 Angle Sensor with Quadrant Photodiode

An angle sensor is a sensor typically for detecting the tilt angle of a surface. Such a sensor with a thin light beam, typically called a surface slope sensor, can also detect surface local slopes. The simplest way to construct an angle sensor is to utilize the method of optical lever. As shown in Figure 1.1, a light beam is projected onto the target surface. The optical spot of the reflected beam on a position photodetector with a distance L from the target will move in the W- and V-directions if the sample tilts about the X- and Y-axes. The two-dimensional components of the tilt angle θ_X and θ_Y can be calculated from the moving distances Δw and Δv of the spot on the photodetector as follows:

$$\theta_X = \frac{\Delta w}{2L}, \tag{1.1}$$

$$\theta_Y = \frac{\Delta v}{2L}. \tag{1.2}$$

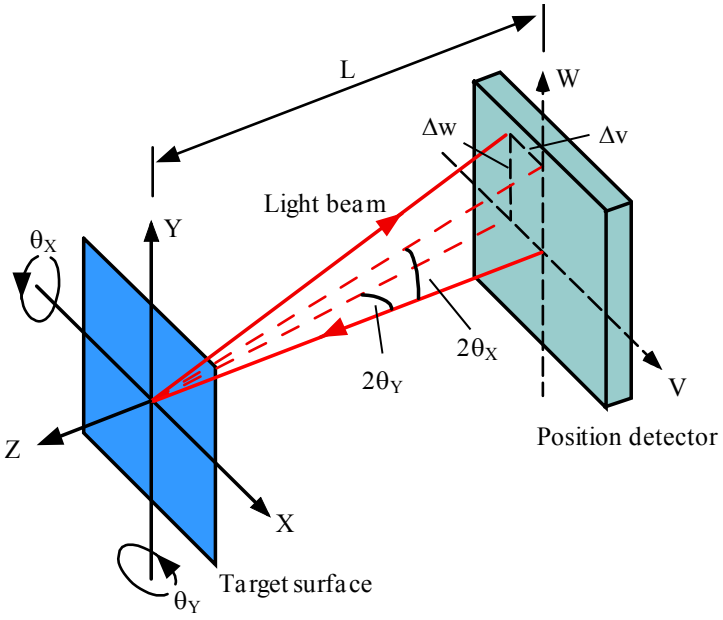

Figure 1.1. Detection of tilt angle by the optical level method

This method is simple but errors arise when distance L changes. This problem can be solved by the technique of autocollimation [7]. As shown in Figure 1.2, an objective lens is placed between the sample and the photodetector. If the photodetector is placed at the focal position of the lens, the relationship between the tilt and the readout of the photodetector becomes:

$$\theta_X = \frac{\Delta w}{2f}, \tag{1.3}$$

$$\theta_Y = \frac{\Delta v}{2f}, \tag{1.4}$$

where f is the focal length of the objective lens. As can be seen in Equations 1.3 and 1.4, the distance between the sample surface and the autocollimation unit composed of the objective lens and the position detector does not affect the angle detection.

In the case of form measurements of precision surfaces and motion measurements of precision stages, the angle of interest is very small and the sensitivity of the angle sensor is required to be very high. The sensitivity of the angle sensor based on autocollimation can be improved by choosing an objective lens with a long focal length. However, this will influence the compactness of the angle sensor. Here, we discuss how to improve the sensitivity of the angle sensor by choosing proper photodetectors without increasing the focal length of the lens.

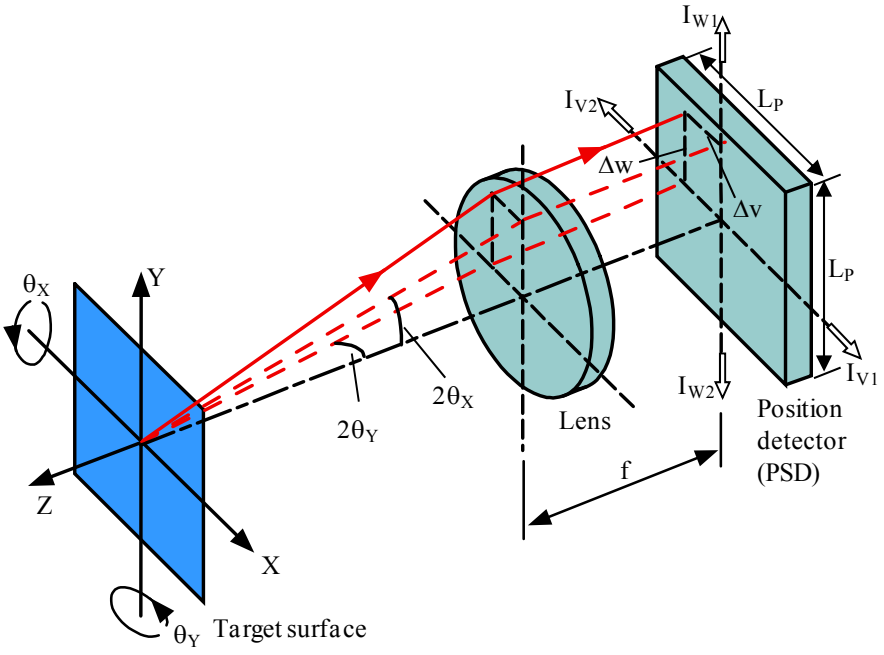

Figure 1.2. Detection of tilt angle by the autocollimation method with a PSD

The linear lateral effect position-sensing device (PSD) is widely used to detect the position of a light spot [8, 9]. PSDs provide continuous position information and have the advantage of good linearity. Position detection is also not affected by the intensity distribution of the light spot. Let the sensitive length of a two-dimensional (2D) PSD be L_P in both X- and Y-directions. The two-dimensional positions Δv and Δw can be obtained from the two-dimensional output $v_{\mathrm{PSD\_out}}$ and $w_{\mathrm{PSD\_out}}$ of the PSD, which are calculated from the photoelectric currents I_{v1}, I_{v2}, I_{w1}, and I_{w2} in Figure 1.2 through the following equations:

$$v_{PSD\_out} = \frac{(I_{v1} - I_{v2})}{(I_{v1} + I_{v2})} \times 100\% = \frac{2}{L_P}\Delta v = \frac{4f}{L_P}\theta_Y , \tag{1.5}$$

$$w_{PSD\_out} = \frac{(I_{w1} - I_{w2})}{(I_{w1} + I_{w2})} \times 100\% = \frac{2}{L_P}\Delta w = \frac{4f}{L_P}\theta_X . \tag{1.6}$$

It can be seen that the sensitivities of a 2D PSD, which are defined as $v_{\mathrm{PSD\_out}}/\Delta v$ (or $x_{\mathrm{PSD\_out}}/\theta_Y$) and $w_{\mathrm{PSD\_out}}/\Delta w$ (or $y_{\mathrm{PSD\_out}}/\theta_X$), respectively, are mainly determined by the sensitive length, and are not adjustable. Since the sensitivities are inversely proportional to the sensitive length, a PSD with a short sensitive length is preferred for obtaining high sensitivity. In Equations 1.5 and 1.6, when an objective lens with a focal length of 40 mm is used, a 0.01 arc-second angle θ_X (or θ_Y) only corresponds to a position change Δw (or Δv) of approximately 4 nm. Assume that the required resolution of the angle sensor is 0.01 arcsec and the dynamic range (measurement range/resolution) is 10,000. The preferred sensitive length of the PSD, which corresponds to the measurement range of the angle sensor, is calculated to be approximately 40 μm. However, commercially available PSDs typically have sensitive lengths of several millimeters, which generate unnecessarily large measurement ranges of angle. Considering the fact that the practical signal to noise ratios (dynamic ranges) of the current/voltage conversion amplifiers used to pick up the photoelectric currents do not easily exceed 10,000, it is difficult to achieve the required resolution of angle detection, which is determined by the measurement range and the dynamic range. Another parameter to determine the resolution of a PSD is the noise current. The noise current level of a 2D PSD is several times larger than that of a one-dimensional (1D) PSD. From this point of view, it is more feasible to use 1D PSDs instead of 2D PSDs. However, two 1D PSDs, with sensitive directions aligned perpendicularly, are necessary for detecting any 2D angle information. This results in a more complicated structure. Misalignment of the sensitive axes of each PSD will also increase the measurement uncertainty. Moreover, just as with a 2D PSD, the resolution of a 1D PSD will not be high enough, where the resolution is basically dominated by the sensitive length and the dynamic range.

Another possible photodetector is the quadrant photodiode (QPD) [10, 11]. As shown in Figure 1.3, a QPD is placed at or slightly apart from the focal point of the objective lens so that a light spot with a width of D_S is generated on the QPD.

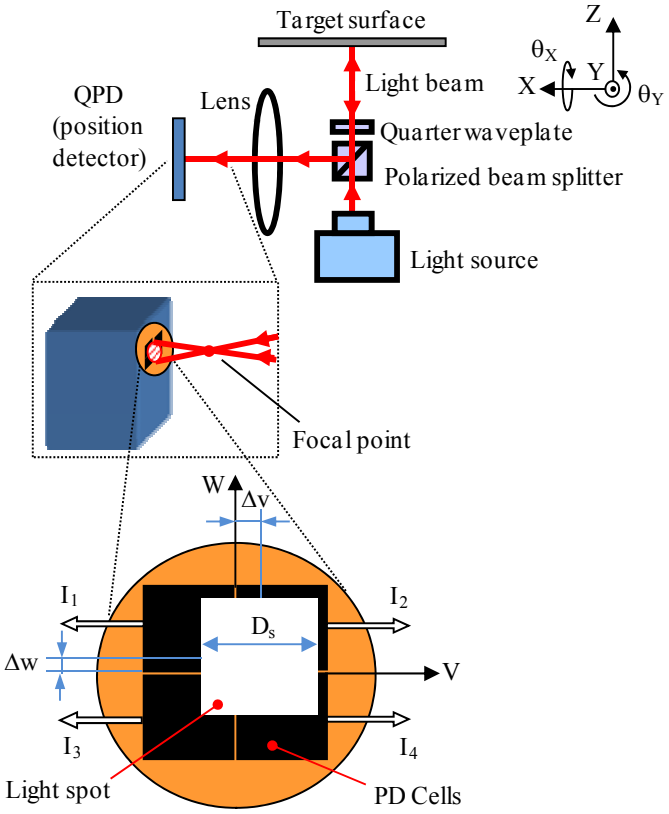

Figure 1.3. The angle sensor of using a QPD

For simplicity, assume the shape of the light spot is rectangular and the intensity distribution of the light spot is uniform. The two-dimensional position of the light spot can be calculated by:

$$v_{QPD\_out} = \frac{(I_1 + I_3) - (I_2 + I_4)}{(I_1 + I_2 + I_3 + I_4)} \times 100\% = \frac{2}{D_s}\Delta v = \frac{4f}{D_s}\theta_Y , \tag{1.7}$$

$$w_{QPD\_out} = \frac{(I_1 + I_2) - (I_3 + I_4)}{(I_1 + I_2 + I_3 + I_4)} \times 100\% = \frac{2}{D_s}\Delta w = \frac{4f}{D_P}\theta_X , \tag{1.8}$$

where I_1, I_2, I_3, I_4 are the photoelectric currents from the QPD cells.

It can be seen that the sensitivity of the QPD for position and/or angle detection is inversely proportional to the width of the light spot on the sensitive window of the QPD. The width of the light spot is a function of the location of the QPD relative to the focal position of the objective lens along the optical axis of the autocollimation unit. A proper measurement range/sensitivity of position and/or angle detection can thus be obtained through adjusting the location of the QPD.

High sensitivity and resolution can be achieved by using this technique. It should be pointed out that if the shape of the light spot were not rectangular but round, the relationships shown in Equations 1.7 and 1.8 would become non-linear. The intensity distribution of the light beam will also influence the linear relationships.

Figure 1.4 shows a schematic view of an angle sensor designed to demonstrate the feasibility of using a QPD as the position photodetector. A laser diode with a wavelength of 780 nm was used as the optical source. The output light from the laser diode unit was a collimated beam with a diameter of 1 mm. An achromatic lens with a short focal length of 40 mm was employed as the objective lens for the sake of compactness. A QPD was used as the photodetector to detect the 2D angle information. Another 1D PSD was also used in the same sensor to detect the 1D angle information about the *Y*-axis so that the sensitivities when using PD and PSD can be compared experimentally. The light beam passing through the objective lens was split into two beams, which were received by the QPD and the PSD, respectively. The PSD has a sensitive length of 2.5 mm, which was the shortest that could be found on the market. The sensor was designed to be within 90 mm (*X*) × 30 mm (*Y*) × 60 mm (*Z*) in size.

Figure 1.5 shows a calibration result of the 2D angle sensor using the QPD. A commercial autocollimator with a resolution of 0.05 arcsec was used as the reference. The target surface in Figure 1.4, which was mounted on a manual tilt stage, can be tilted manually about the *X*-axis and *Y*-axis, respectively. The tilt angle was detected by the angle sensor and the autocollimator simultaneously. The horizontal axes show the applied tilt angles measured by the autocollimator in arcseconds, and the vertical axes show the outputs of the angle sensor in percentages, which are defined in Equations 1.7 and 1.8. As can be seen in Figure 1.4, the angle sensor using a QPD has the ability to detect the two-dimensional tilt angle in a range of approximately 200 arcsec.

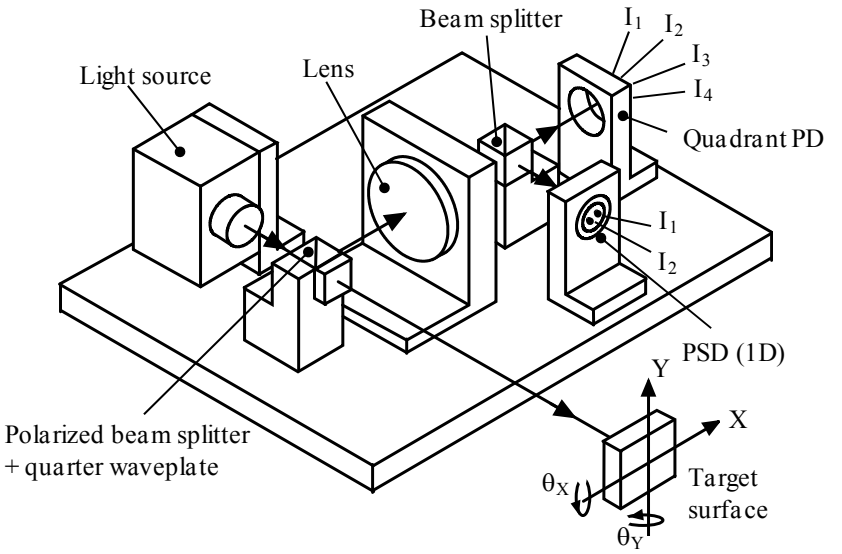

Figure 1.4. An angle sensor with a QPD and a one-dimensional PSD

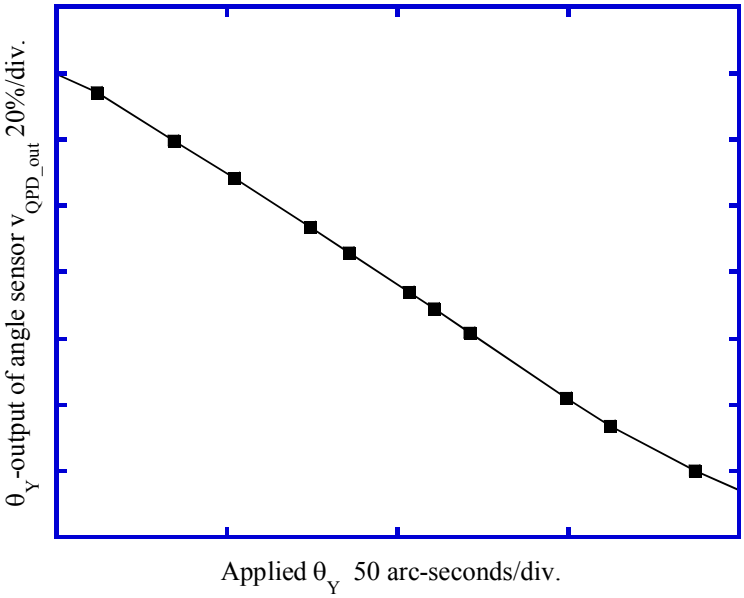

(a) θ_X

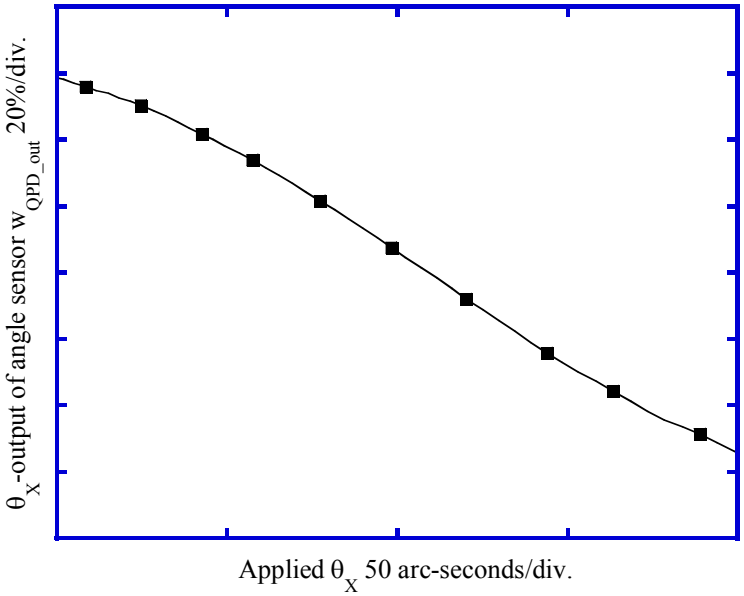

(b) θ_Y

Figure 1.5. Calibration of the angle sensor with a QPD

Figure 1.6 shows a comparison of the sensor output when using the QPD and the 1D PSD. Since the 1D PSD can only detect the tilt about the *Y*-axis, the comparison was made only with the *V*-directional output of the QPD. Note that the two vertical scales in the graph are ten times different from each other. It can be seen that the sensitivity when using the QPD is approximately 30 times higher than that when using the PSD.

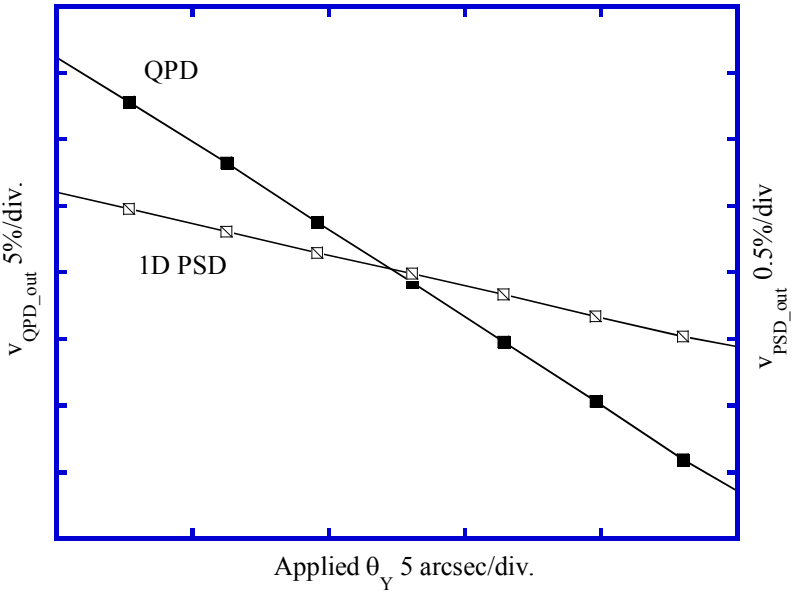

Figure 1.6. Comparison of the angle sensor outputs when using QPD and PSD

The angle sensor with a QPD was employed for measurement of the tilt error motions about the *Y*-axis (yawing) and the *X*-axis (pitching) of an aerostatic bearing linear stage (air-slide) with its axis of motion along the *Z*-direction. Figures 1.7 and 1.8 show the measurement results and the experimental setup, respectively. For comparison, the tilt error motions were also measured by a commercial autocollimator with a resolution of 0.1 arc-second simultaneously. The mirrors for the angle sensor and the autocollimator were mounted on the moving table of the stage. The moving table was first moved 50 mm forward, then kept stationary, then finally moved 50 mm back to the starting point. As can be seen in Figure 1.7, the stage was measured to have a yawing error motion and a pitching error motion of approximately 1 arc-second during the forward motion. The tilt error motions were associated with the acceleration of the moving table of the stage. When the moving table was kept stationary, the tilt error motions of the moving table were on the order of 0.1 arc-second, which were approximated to be one tenth of those during acceleration. When the moving table was moved back, the tilt error motions had the same amplitude as those during the forward motion but with a different tilt direction. This corresponds to the difference of directions between the forward driving force and the backward driving force from the motors. The angle sensor also showed a lower noise level compared with the autocollimator.

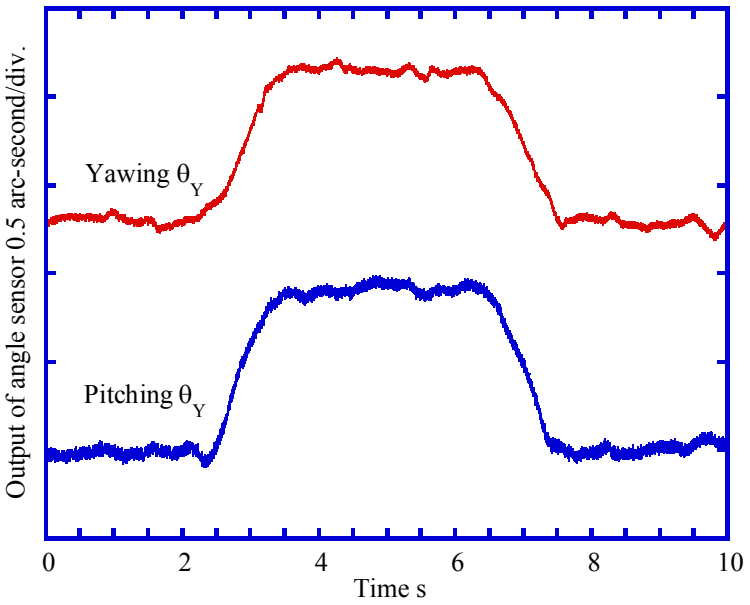

(a) Results from the angle sensor with a QPD

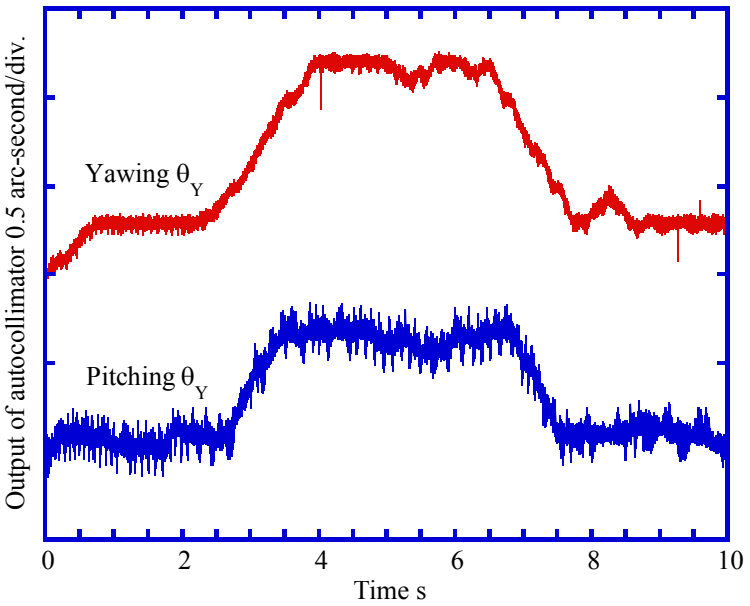

(b) Results from the autocollimator

Figure 1.7. Measurement of tilt error motions by using the angle sensor and a commercial autocollimator

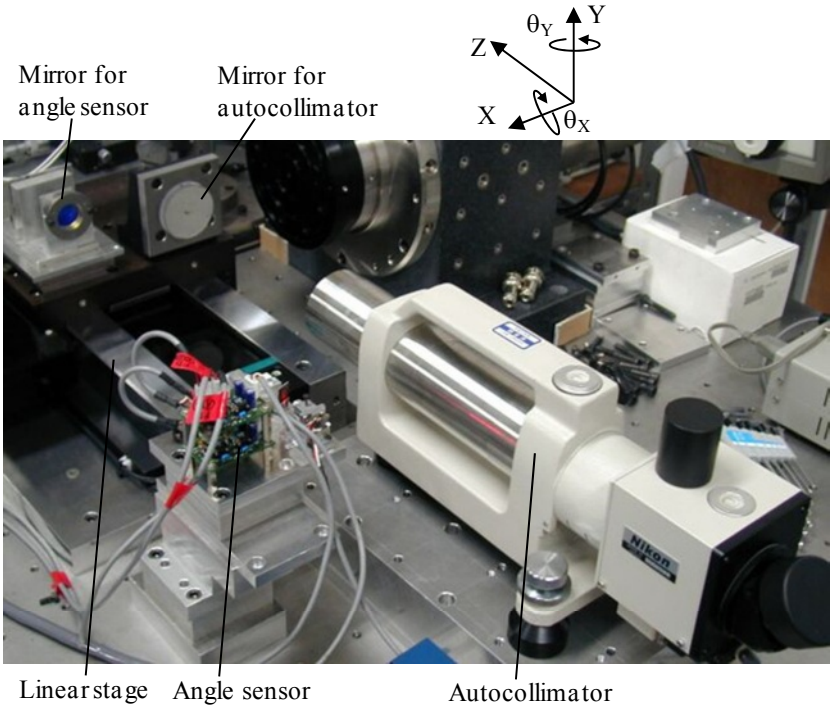

Figure 1.8. Experimental setup for measurement of stage tilt motions

The angle sensor can also be used as a slope sensor for detection of surface local slopes [12–16]. Figure 1.9 shows a schematic of the scanning system for measurement of a silicon wafer substrate by using a slope sensor. The system consists of a wafer spindle, a 2D slope sensor and a linear stage. The spindle axis is along the *Z*-axis and the linear stage moves along the *X*-axis. The slope sensor detects the 2D surface slopes about the *X*- and *Y*-axes.

The coordinates of sampling points on the wafer surface are shown in Figure 1.10. The sampling positions in the *X*-direction are numbered as x_i (i = 1, …, M). At each sampling position x_i, the 2D surface local slopes at points along a concentric circle are detected by the slope sensor. The sampling positions along the circle are numbered as θ_j (j = 1, …, N). The *Y*-output $\mu_Y(x_i, \theta_j)$ can be expressed by

$$\mu_Y(x_i,\theta_j) = f'_Y(x_i,\theta_j) + e_{CX}(x_i) + e_{SX}(x_i,\theta_j)\,, \tag{1.9}$$

where $e_{CX}(x_i)$ is the roll error of the sensor carriage, and $e_{SX}(x_i, \theta_j)$ is the tilt motion component of the wafer spindle about the *X*-axis. The term $f'_Y(x, \theta)$ is the *Y*-directional local slope of the wafer surface, which is defined as:

$$f'_Y(x,\theta) = \partial f(x,\theta)/\partial y\,. \tag{1.10}$$

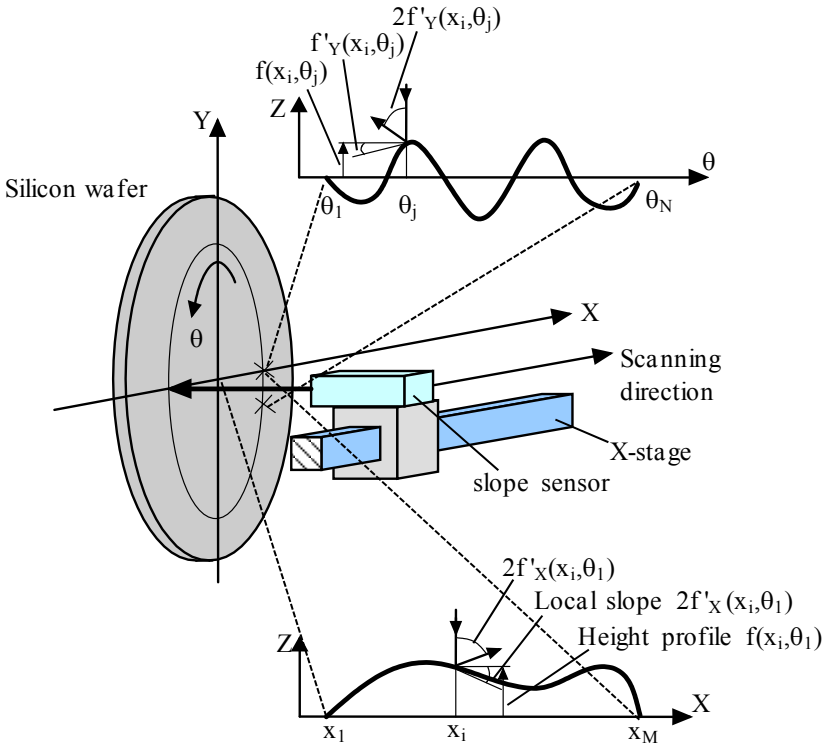

Figure 1.9. Scanning the local slope profile of a silicon wafer by using a slope sensor

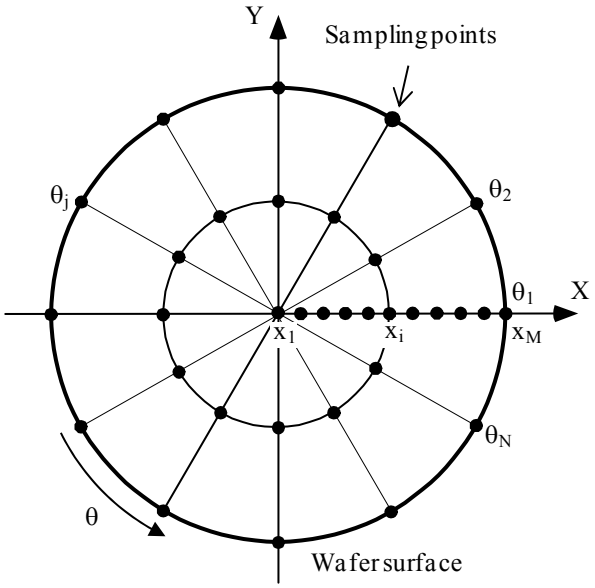

Figure 1.10. Sampling points on the wafer surface

Assuming that the roll error of the sensor stage and the tilt motion of the spindle are small enough or pre-compensated gives

$$\mu_Y(x_i,\theta_j) = f'_Y(x_i,\theta_j)\,. \tag{1.11}$$

For a fixed x_i ($i = 2, \ldots, M$), the height profile $f(x_i, \theta_j)$ of the wafer section along the ith concentric circle can then be calculated from

$$f(x_i,\theta_j) = \sum_{t=2}^{j} \mu_Y(x_i,\theta_t)(\theta_t - \theta_{t-1})x_i + f(x_i,\theta_1)\,, j = 2, \ldots, N, \tag{1.12}$$

where $f(x_i, \theta_1)$ ($i = 2, \ldots, M$) are the profile heights along the X-axis.

To obtain the entire profile of the wafer surface from profiles $f(x_i, \theta_j)$ along a concentric circle in Equation 1.12, the X-outputs of the slope sensor are used to determine the values of $f(x_i, \theta_1)$ ($i = 1, \ldots, M$). The X-outputs of the slope sensor $\mu_X(x_i, \theta_1)$, which correspond to the tilt about the Y-axis, can be expressed by:

$$\mu_X(x_i,\theta_1) = f'_X(x_i,\theta_1)\,. \tag{1.13}$$

The yaw error of the sensor carriage is assumed to be small enough or pre-compensated. The term $f'_X(x, \theta)$ is the X-directional local slope of the wafer surface, which is defined as:

$$f'_X(x,\theta) = \partial f(x,\theta)/\partial x\,. \tag{1.14}$$

The sectional profile $f(x_i, \theta_1)$ along the radial direction can thus be calculated from:

$$f(x_i,\theta_1) = \sum_{t=2}^{i} \mu_X(x_t,\theta_1)(x_t - x_{t-1})\,,\ f(x_1,\theta_1) = 0\,,\ i = 2, \ldots, M. \tag{1.15}$$

The entire surface profile (height map) of the silicon wafer can be obtained by combining the two results in Equations 1.12 and 1.15.

Figure 1.11 shows the experimental system. The wafer was vertically vacuum-chucked on an air-spindle with a rotary encoder and the slope sensor was mounted on a linear motor-driven air-slide with a linear encoder. The spindle and the slide were controlled by a personal computer via RS-232C. The sensor outputs were taken into the PC via a 16-bit AD converter. The sampling positions were determined by the rotary encoder and the linear encoder. A polished silicon wafer substrate with a diameter of 300 mm was used as the specimen. Figure 1.12 shows the outputs of the slope sensor along the circumference direction and the radial direction, which are called the slope maps, respectively. Figure 1.13 shows the evaluated height profile based on Equations 1.12 and 1.15. The out-of-flatness of the wafer was measured to be approximately 10.7 μm.

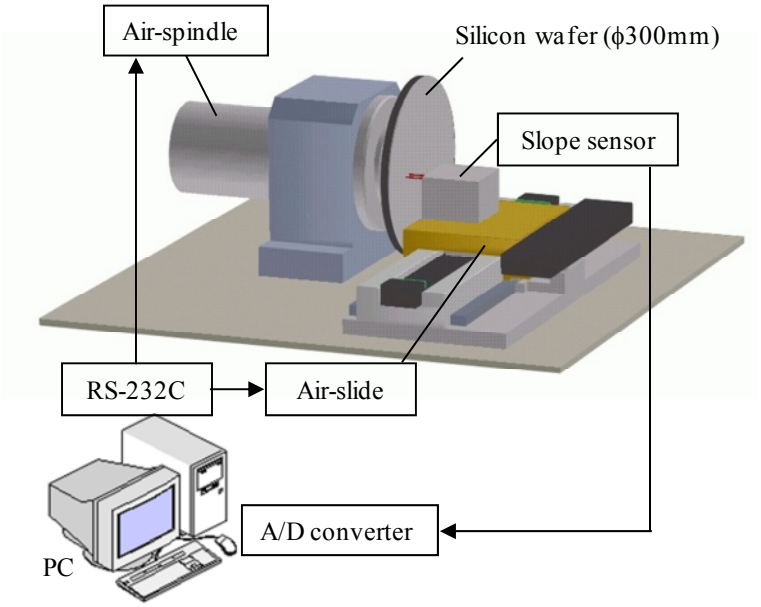

(a) Schematic drawing

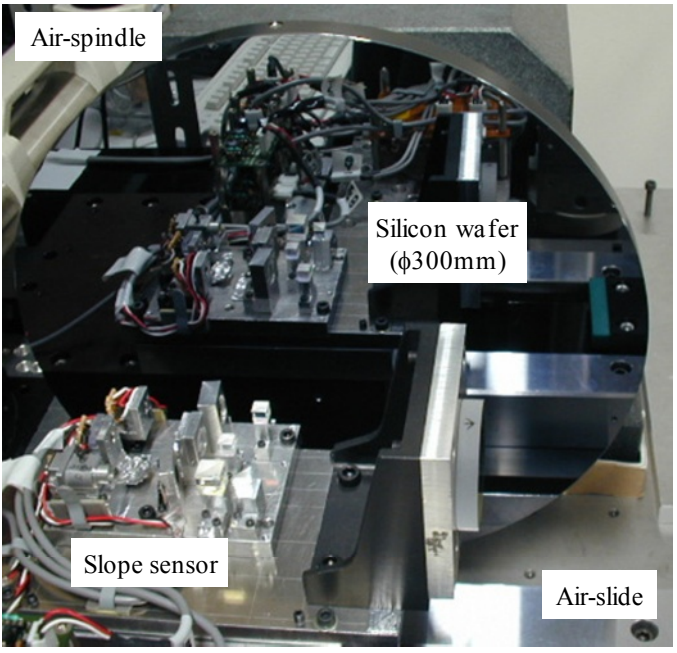

(b) Photograph

Figure 1.11. Experimental system for silicon wafer flatness

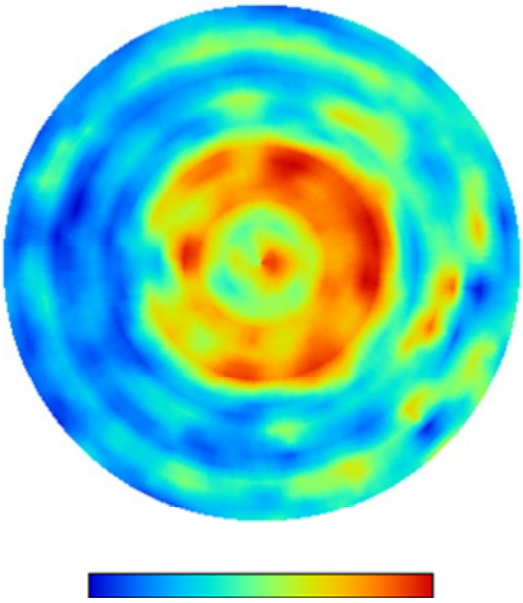

(a) Circumference direction

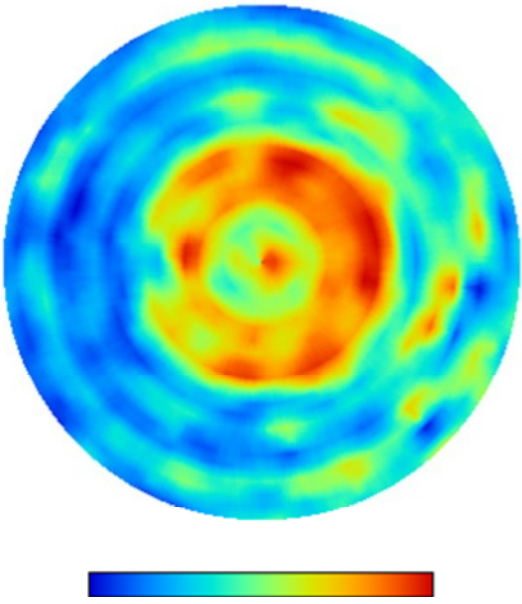

(b) Radial direction

Figure 1.12. Measured slope maps of the wafer surface

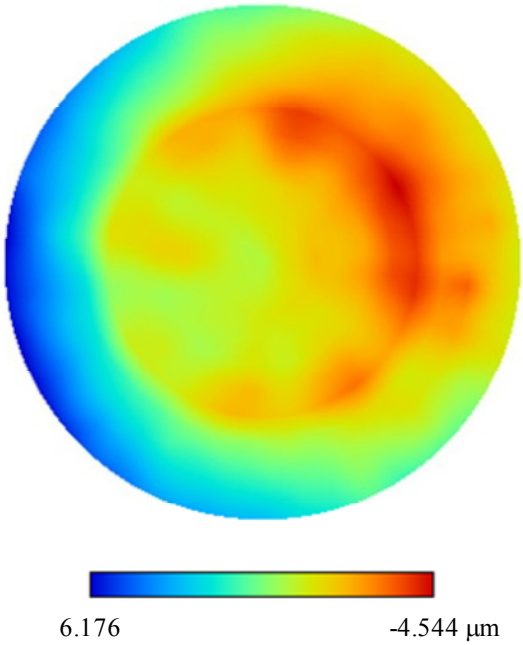

Figure 1.13. Measured height map (out-of-flatness) of the silicon wafer

1.3 Angle Sensor with Photodiode Array

As described in Section 1.2, in the case of using a quadrant photodiode or a bi-cell photodiode, both the resolution and the range of angle measurement are determined by the light spot size on the photodiode. The smaller the spot size, the higher the resolution but the smaller the range. Obtaining a higher resolution means a reduction of range, which is a problem for measurements with large angle variations. This section presents an angle sensor employing a multi-cell photodiode array [17] instead of the bi-cell PD or quadrant PD to achieve a larger measurement range while maintaining the resolution.

Figure 1.14 shows a schematic of the angle sensor with a one-dimensional (1D) multi-cell PD array for the measurement of the tilt angle of θ_Y. The basic structure is the same as that shown in Section 1.2. A multi-cell PD array is placed at the focal position of the objective lens to detect the V-directional displacement Δv of the light spot at the focal plane. Multiple PD cells of the multi-cell PD array are aligned along the V-direction in the VW-plane. The origin of the V-axis as well as the initial position of the light spot is located in the center of the gap between cells 1 and 2.

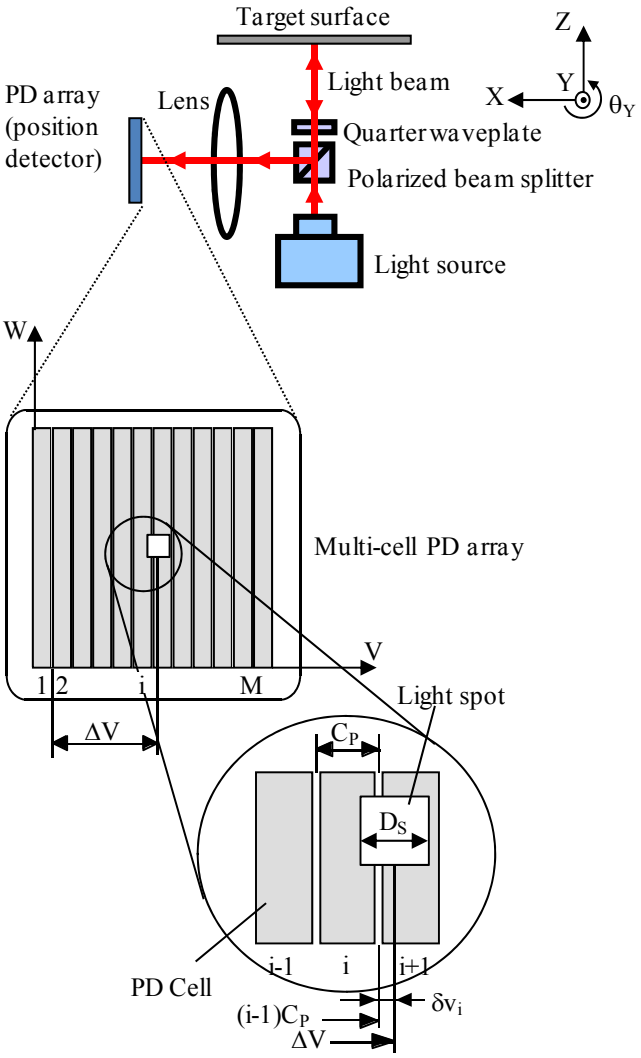

Figure 1.14. The angle sensor using a multi-cell PD array

Assume that the width of each cell is C_P and the total number of cells is M. If the light spot resides on cells i and $i + 1$, the position δv_i of the light spot relative to the center of the gap between cells i and $i + 1$ can be obtained from the following equation, based on the position-sensing principle of a bi-cell PD:

$$\delta v_i = \frac{I_{i+1} - I_i}{I_{i+1} + I_i} \cdot \frac{D_S}{2}, \; i = 1, \ldots, M-1, \tag{1.16}$$

where I_i and I_{i+1} are the photoelectric currents of cells i and $i + 1$, respectively, and D_S is the diameter of the light spot. For the sake of clarity, the non-linearity caused by the non-rectangular shape of the light spot is ignored. The width of the gap is also not considered. As can be seen from Equation 1.16, the sensitivity and range of measuring δv_i are determined by the diameter of the light spot. It is necessary to reduce D_S in order to obtain a higher resolution, but this will result in a reduction of range.

To improve both the resolution and the range, the cell width C_P is designed to be equal to or slightly smaller than the diameter D_S. In this case, D_S can be replaced with C_P in Equation 1.16. In addition, when the light spot moves across the multi-cell PD along the V-direction, the light spot will reside on two cells at any position within the sensitive area of the PD so that the position ΔV can be obtained by

$$\Delta V = (i-1)C_P + \delta v_i \,, \tag{1.17}$$

$$\theta_Y = \frac{\Delta V}{2f} = \frac{(i-1)C_P + \delta v_i}{2f} = \frac{(i-1)C_P}{2f} + \Delta\theta_{Yi} \,, \; i = 1, \ldots, M-1, \tag{1.18}$$

where $\Delta\theta_{Yi}$ is the angle component detected by cells i and $i + 1$, which corresponds to a conventional bi-cell PD.

$$\Delta\theta_{Yi} = \frac{\delta v_i}{2f} = \frac{I_{i+1} - I_i}{I_{i+1} + I_i} \cdot \frac{C_P}{4f} = V_{Array\_out\_i} K_\theta \,, \; i = 1, \ldots, M-1, \tag{1.19}$$

where $V_{\text{Array\_out\_}i}$ shows the relative variation of the sensor output, and K_θ corresponds to the sensitivity of angle detection. Then,

$$V_{Array\_out\_i} = \frac{I_{i+1} - I_i}{I_{i+1} + I_i} \times 100\% \,, \tag{1.20}$$

$$K_\theta = \frac{C_P}{4f} \,. \tag{1.21}$$

Consequently, the angle measurement range can be improved by M–1 times while maintaining the resolution compared with a bi-cell PD. The constant K_θ can be determined by a calibration process. D_S is determined by the numerical aperture and the aberration of the objective lens. Figure 1.15 shows a photograph of the angle sensor developed for testing the PD array. The diameter of the beam projected onto the target mirror was 0.8 mm and the focal length of the objective lens was 30 mm. The numerical aperture was calculated to be 0.027. Figure 1.16 shows the intensity distribution of the light spot on the focal plane of the objective lens, which was detected by a beam profiler. The light spot had a typical Gaussian distribution. The diameter D_S of the light spot was approximately 50 μm.

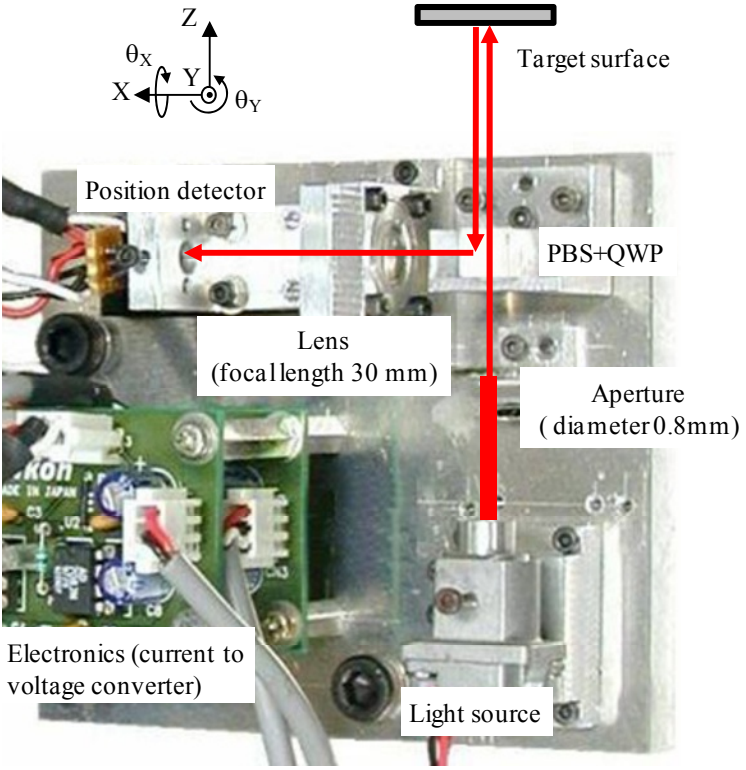

Figure 1.15. Photograph of the angle sensor

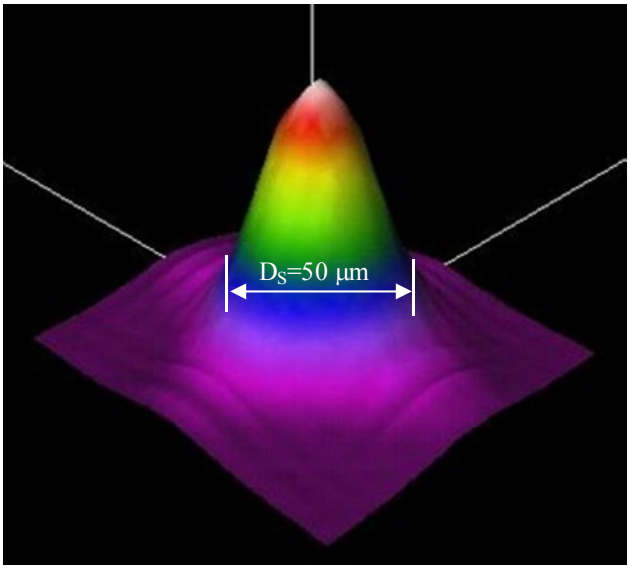

Figure 1.16. Intensity distribution of the focused light spot

On the other hand, however, commercial PD arrays have large cell widths, on the order of 1 mm, and large gaps between cells, on the order of 100 μm, which are not suited for use in the precision angle sensor. A multi-cell PD array was thus specifically designed and fabricated. Figure 1.17 shows the geometry of the sensitive area of the PD array. The pitch between the cells, which is the sum of the gap between cells and the width of each cell, was determined based on the measurement result of the diameter of the focused light spot (D_S) shown in Figure 1.16. The gap between cells was designed to be 5 μm based on the facility capability. The width of each PD cell was designed to be 40 μm so that the sum of the cell width and twice the gap was equal to the spot diameter. The angle range detected by two adjacent cells was calculated to be 156 arcsec. The number of cells was designed to be 16 and the total range of angle detection by the PD array was 2340 arcsec. The cell length, which was not a critical factor, was designed to be 1 mm for ease of alignment. The rectangular contact hole was 20 μm in length. The width of the aluminum electrode and wire was 40 μm, which was the same as the cell width. The wires of two adjacent PD cells were connected to different ends of the cells to avoid contact between the wires.

Figure 1.18 shows the process chart for fabricating the PD array. Figure 1.19 shows the 1D PD array with electrodes. Figures 1.20 and 1.21 show photographs of the sensitive area in the fabricated one-dimensional PD array and the circuit board for mounting the PD array.

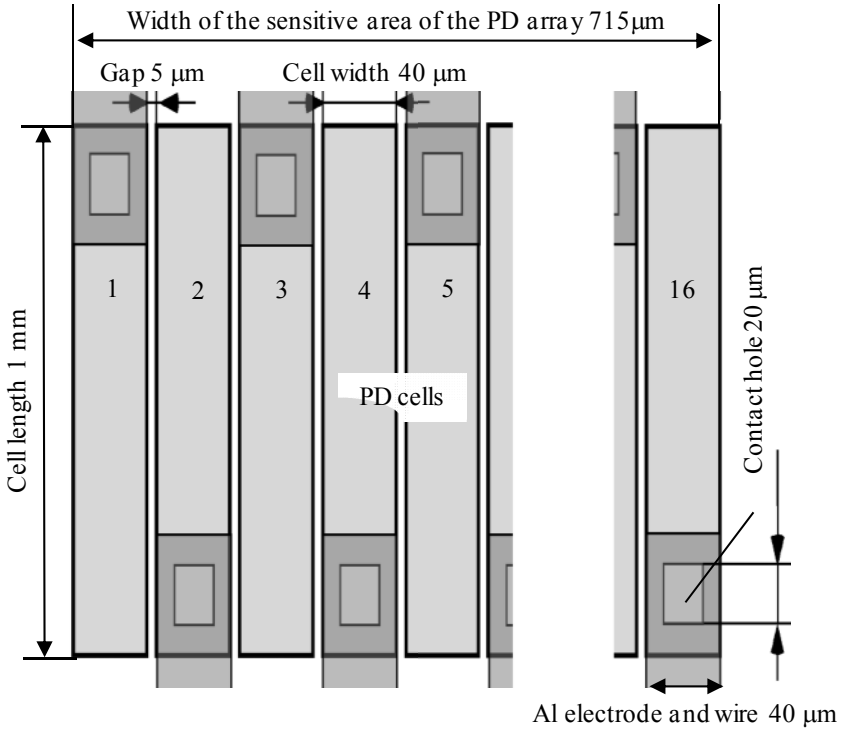

Figure 1.17. Geometric design of the multi-cell PD array

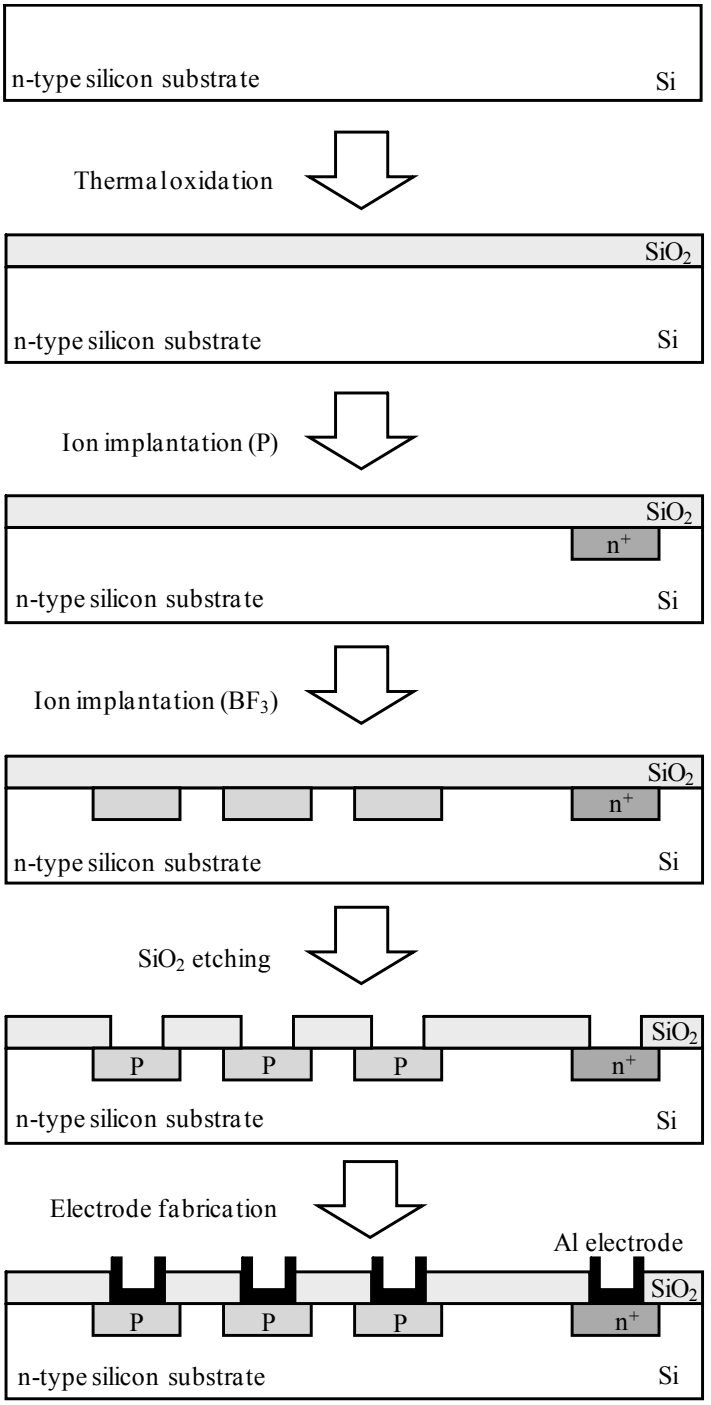

Figure 1.18. Process chart of the multi-cell PD array

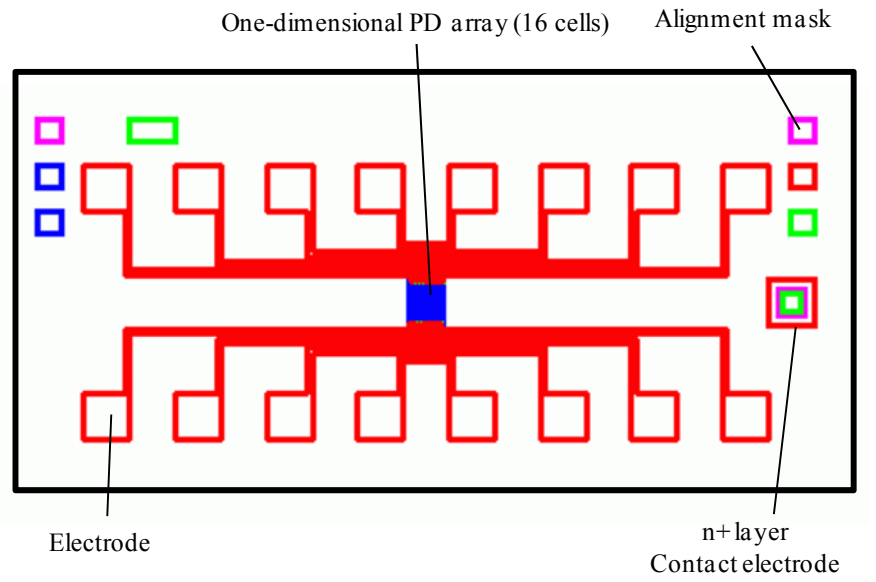

(a) Schematic drawing

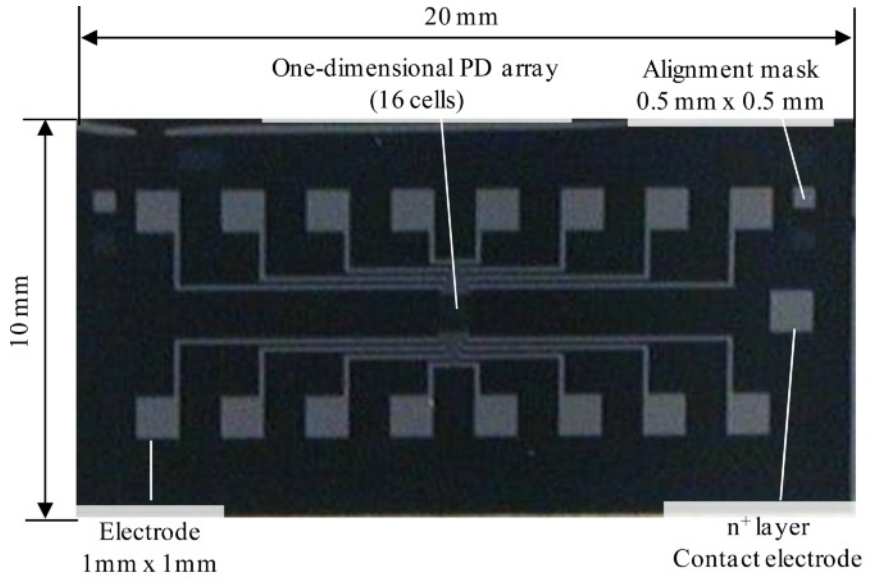

(b) Photograph

Figure 1.19. The 1D PD array with electrodes

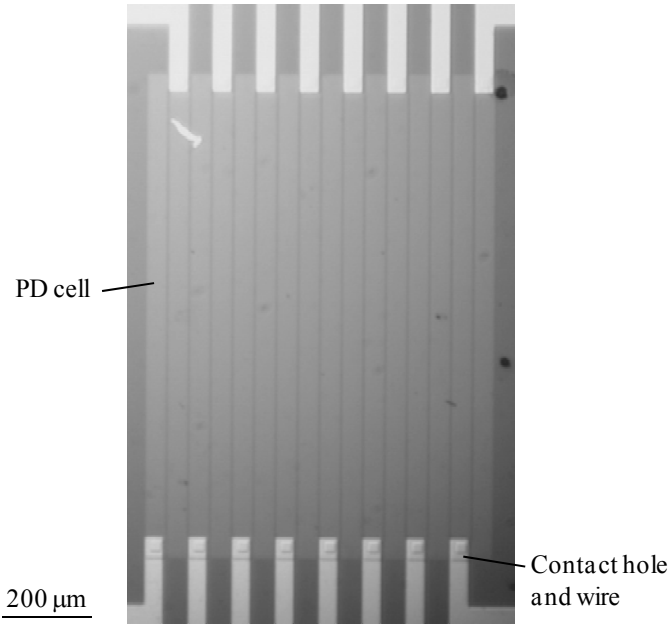

Figure 1.20. Photograph of the sensitive area of the 1D PD array

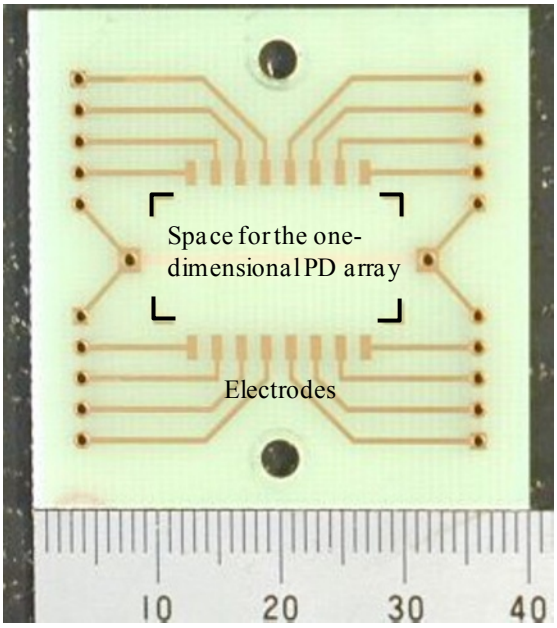

Figure 1.21. Photograph of the circuit board for mounting the 1D PD array

Experiments were conducted to test the angle sensor employing the multi-cell array as the light position detector. As can be seen in Figure 1.22, two mirrors, one for the angle sensor and the other for a commercial autocollimator, were mounted on a tilt stage. The tilt angle θ_Y of the tilt stage was detected by the angle sensor and the autocollimator simultaneously for comparison. The autocollimator had an objective lens with a focal length of 430 mm. The resolution and range were 0.1 and 1200 arcsec, respectively. The dimension was 440 mm (L) × 80 mm (W) × 146 mm (H).

Figures 1.23 and 1.24 show the results of the resolution test where a PZT-driven tilt stage was employed. In the test shown in Figure 1.23, the stage was tilted periodically with an amplitude of approximated 0.3 arcsec. Considering the slow response of the autocollimator, a 0.5 Hz signal was applied to the PZT stage. As can be seen in the figure, the angle sensor responded much better than the autocollimator, indicating that the angle sensor had a higher resolution. The variations in the amplitudes of the sensor output were caused by the instability in the tilt motion of the stage with an open-loop control. Figure 1.24 shows the result when the amplitude was reduced to approximately 0.02 arc-second. The signal frequency was also increased to 50 Hz. The autocollimator could not detect such a small tilt angle but the output of the angle sensor still followed the tilt motion quite well. The resolution of the angle sensor was evaluated to be approximately 0.01 arc-second. The bandwidth of the angle sensor, which was mainly determined by the sensor electronics, was set to be approximately 1.6 kHz.

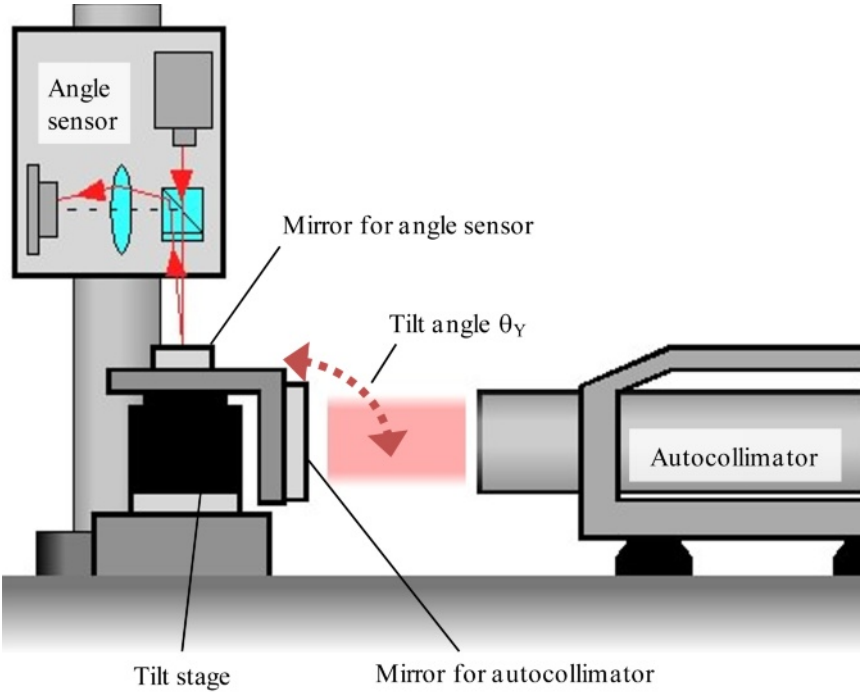

Figure 1.22. Experimental setup for angle detection

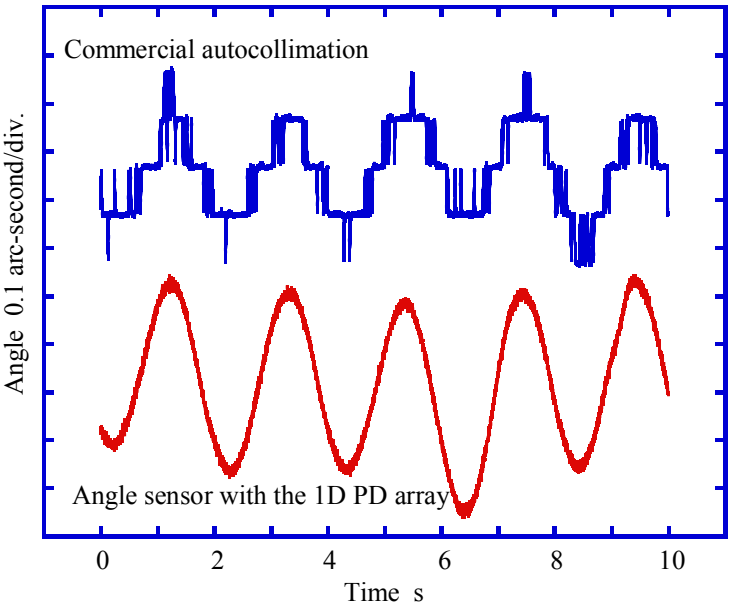

Figure 1.23. Comparison with the commercial autocollimator

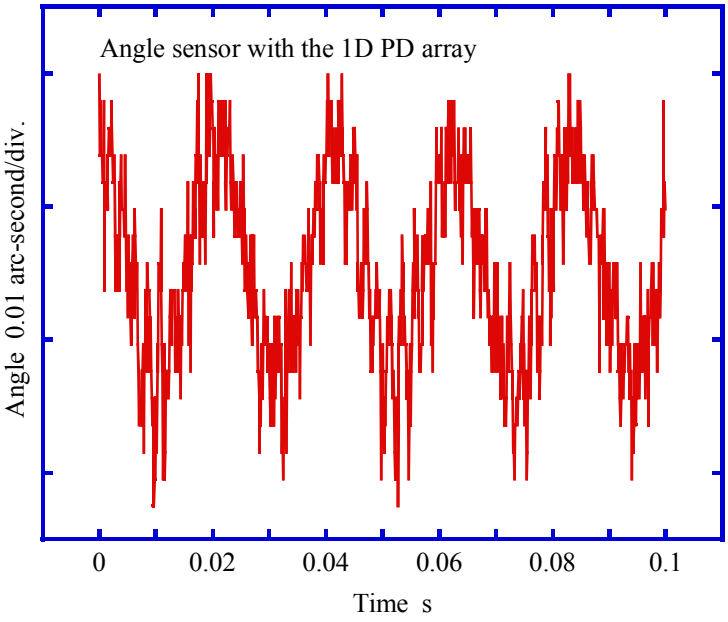

Figure 1.24. Resolution of the angle sensor with the one-dimensional PD array

Figure 1.25 shows the result of testing the measurement range of the angle sensor. A stepping motor-driven tilt stage with a larger tilting range (5º) and a resolution of 1 arc-second was employed instead of the PZT-driven tilt stage shown in Figure 1.22 because the movement range of the PZT-driven tilt stage was smaller than the measurement range of the angle sensor with the PD array. The stage was tilted in such a way that the light spot moved across the PD array from cell 1 to 16. The photoelectric currents of adjacent pairs of PD cells were used to calculate $V_{\text{Array\_out\_}i}$ in Equation 1.20, which was the relative sensor output. As can be seen in Figure 1.25, the tilt angle can be evaluated by each pair of the adjacent PD cells and the measurement range was improved to approximately 2300 arcsec through employing all of the 16 cells.

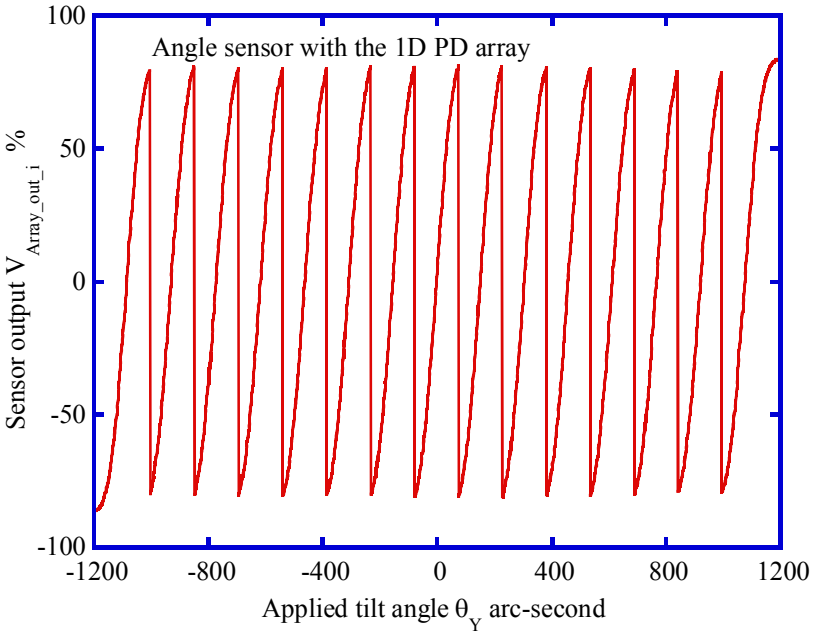

Figure 1.25. Output of the angle sensor with the one-dimensional PD array

The output $V_{\text{Array\_out\_8}}$ from cells 8 and 9 is shown in Figure 1.26. The range of $V_{\text{Array\_out\_8}}$ was 155 arcsec. The non-linearity due to the circular beam cross-section was approximately 27 arcsec. For comparison, a commercial bi-cell PD was also used in the same angle sensor. The cell width was 300 μm, which was much larger than the 50 μm spot diameter. The gap between cells was 10 μm. The sensor output shown in Figure 1.27 corresponds to that defined in Equation 1.7. It can be seen in Figure 1.27 that the effective range was almost the same as that shown in Figure 1.26, indicating that the range is basically determined by the spot size for a bi-cell PD. The non-linearity over an effective range of 160 arcsec was approximately 32 arcsec.

Figure 1.28 shows a fabricated two-dimensional (2D) PD array with 4 × 4 PD cells. Both the tilt angles θ_Y and θ_X can be detected by using the 2D PD array.

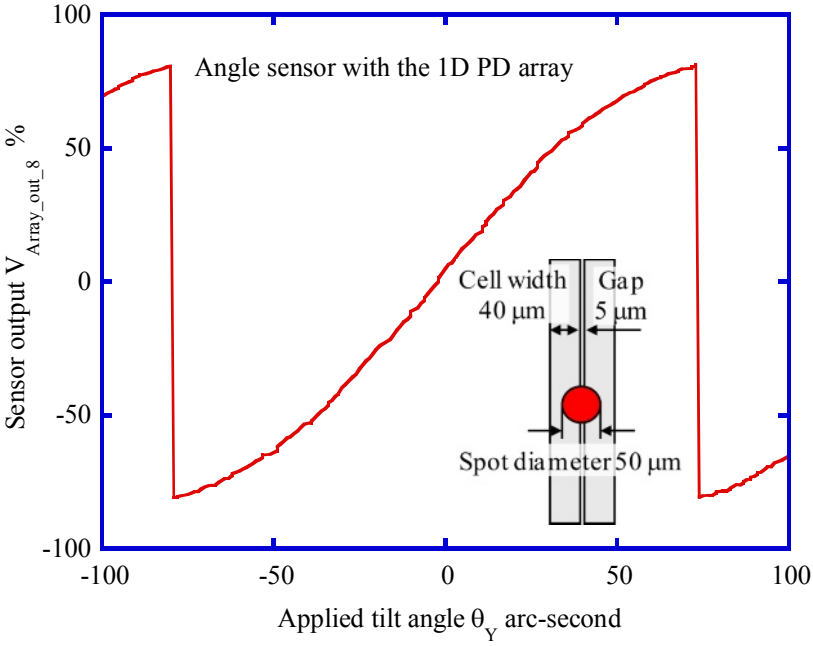

Figure 1.26. Angle sensor output between two adjacent PD cells of the 1D PD array

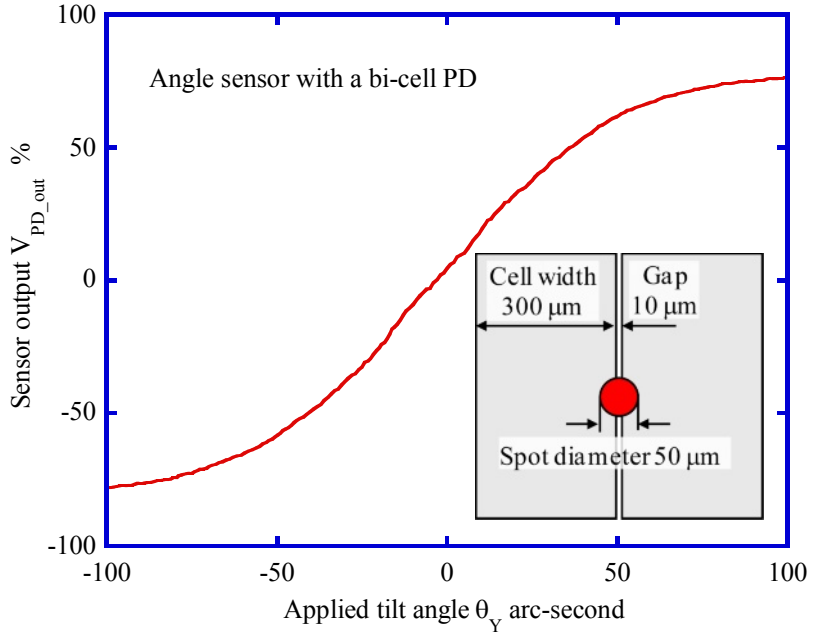

Figure 1.27. Angle sensor output between with a bi-cell PD

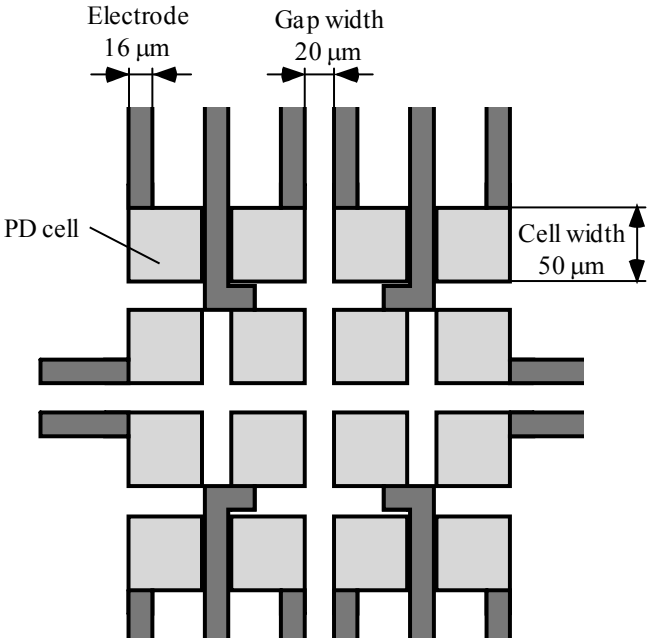

(a) Geometry

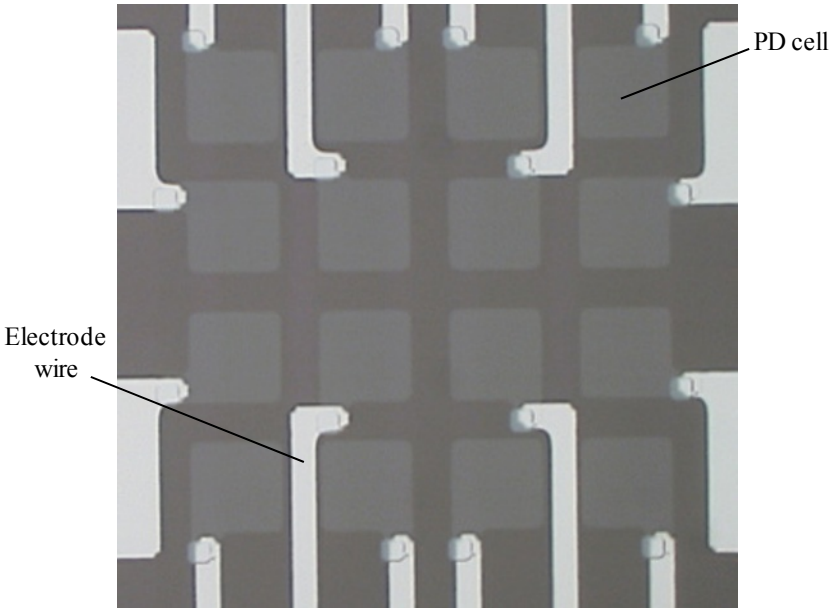

(b) Picture

Figure 1.28. A fabricated 2D PD array

1.4 Angle Sensor with Single-cell Photodiode

As shown in the previous sections, in the case of using a quadrant photodiode or a bi-cell photodiode in an angle sensor, the size of the light spot on the QPD is related to the sensitivity of QPD as well as the angle sensor. The smaller the size of the light spot, the higher the sensitivity. It is thus effective to reduce the light spot size for improvement of the sensor sensitivity. However, there are gaps between the PD cells, which are not sensitive to the light spot. The minimum light spot size as well as the sensor sensitivity is thus limited by the gap size between the photodiode cells of the QPD. This section presents an angle sensor using single-cell photodiodes instead of the QPD as the light position detector so that the limitation caused by the insensitive gaps between PD cells of the QPD can be overcome. In the sensor, the light spot size can be reduced to the diffraction limit for realizing a higher sensitivity of angle detection.

Figure 1.29 shows the schematic of the angle sensor using single-cell photodiodes. There are three single-cell photodiodes. PD1 and PD2 are employed for detection of the tile angle components θ_Y and θ_X, respectively. PD3 is employed to monitor the variation of the intensity of the reflected beam. Assume that the beam diameter and the intensity of the light beam received by PD3 are D_0 and INT_0, respectively. The diameter and intensity of the light beams received by PD1 and PD2, which are placed at the focal position of the lens, are D_S and $INT_0/2$, respectively.

As can be seen in Figure 1.29, a tilt motion θ_Y about the Y-axis will cause a displacement of Δv for the light spot on PD1. Similarly, a tilt motion θ_X about the X-axis will cause a displacement of Δw for the light spot on PD2. Assume that the sensitive area of PD0 is large enough so that the light spot on PD0 does not move out of the sensitive area. The output currents of the photodiodes can be expressed by:

$$I_0 \approx C_{on} INT_0 , \tag{1.22}$$

$$I_1 \approx C_{on} \frac{INT_0}{2D_s} \Delta v = C_{on} \frac{INT_0}{D_s} f\theta_Y , \tag{1.23}$$

$$I_2 \approx C_{on} \frac{INT_0}{2D_s} \Delta w = C_{on} \frac{INT_0}{D_s} f\theta_X , \tag{1.24}$$

where C_{on} is the coefficient of converting the light intensity to current of the photodiode. The outputs of the angle sensor, in which INT_0 is removed, can be described as:

$$v_{SPD\_out} = \frac{I_1}{I_0} \times 100\% = \frac{f}{D_s} \theta_Y , \tag{1.25}$$

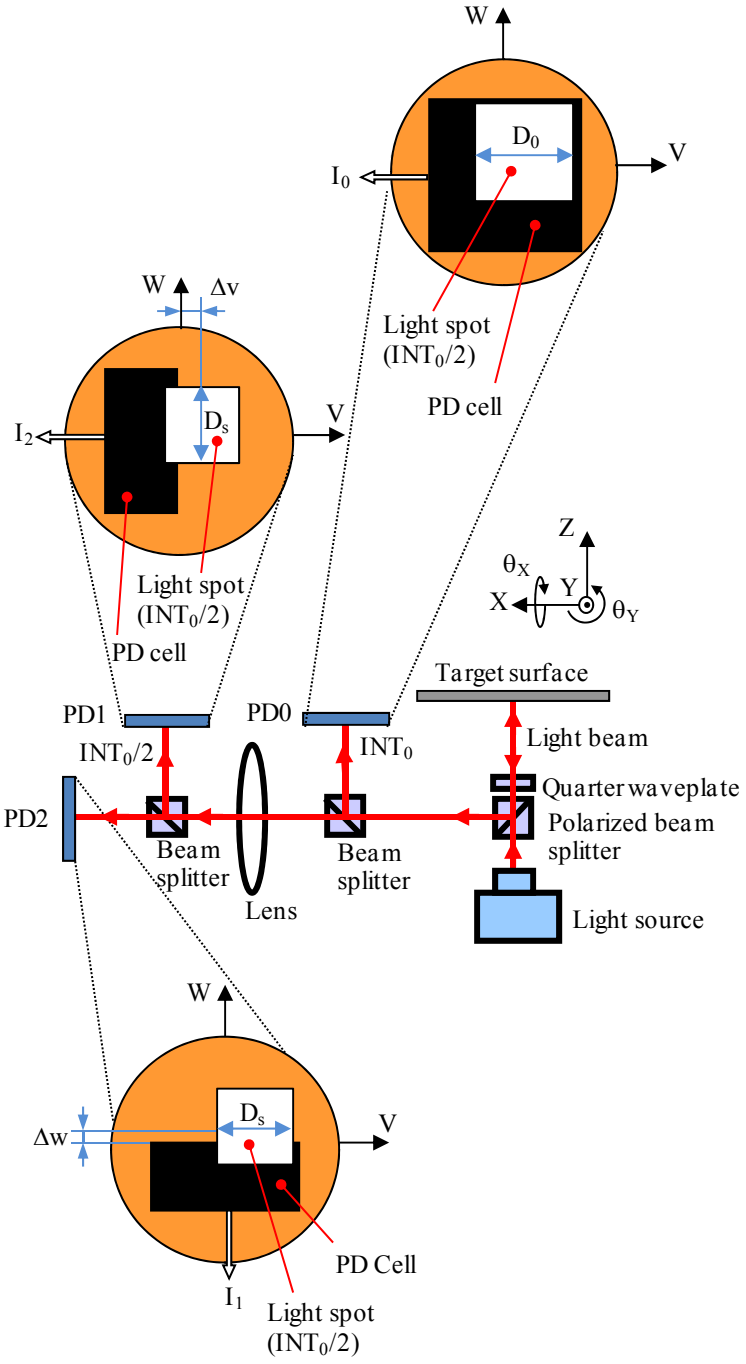

Figure 1.29. Schematic of an angle sensor with single-cell photodiodes

$$w_{SPD\_out} = \frac{I_2}{I_0} \times 100\% = \frac{f}{D_s}\theta_X . \tag{1.26}$$

Rewriting Equations 1.25 and 1.26 gives

$$\theta_Y = K_{S\theta} v_{SPD\_out} , \tag{1.27}$$

$$\theta_X = K_{S\theta} w_{SPD\_out} , \tag{1.28}$$

where

$$K_{S\theta} = \frac{D_s}{f} \tag{1.29}$$

is referred to as the sensitivity for angle detection.

Figure 1.30 shows a photograph of the angle sensor using single-cell photodiodes. In Figure 1.29, PD1 and PD2 share the same lens for simplicity of

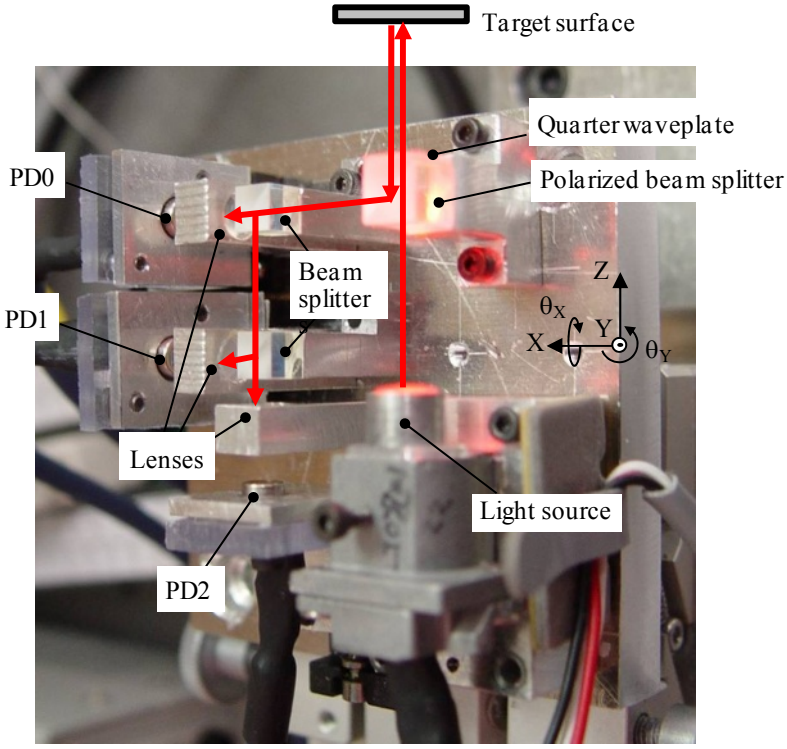

Figure 1.30. Photograph of the angle sensor with single-cell photodiodes

description. Because it is necessary to use a short focal length of lens for generation of a small D_S, two identical lenses were employed for PD1 and PD2 in Figure 1.30. Another lens was placed in front of PD0 for reducing the diameter D_0. The light source was a laser diode with a wavelength of 685 nm. The diameter from the light source was approximately 5 mm. The focal length of the lenses was 7.5 mm. The size of the sensitive area of each photodiode was 1.1 mm × 1.1 mm. The diameter of the light spot D_S was calculated to be approximately 1.25 μm based on the theory of light diffraction. This value was smaller than the 10 μm gap of the QPD used in Section 1.2 and cannot be used in an angle sensor with a QPD.

Figure 1.31 shows the experimental results. The sensitivity $K_{S\theta}$ was approximately 3% / arc-second. It can be seen that the sensor using single-cell photodiodes has a much higher sensitivity than the angle sensor using QPD as shown in Figure 1.5.

1.5 Summary

Angle sensors using different types of photodiodes as light position detectors have been presented. The method of using a quadrant PD was first discussed. It has been confirmed that the diameter of the light spot focused on the QPD is a critical factor to determine the range and sensitivity for angle detection. A smaller light spot can generate a higher sensitivity but reduce the measurement range.

The second method employs a multi-cell PD array as the light position detector. This method can improve the measurement range without reducing the resolution based on the fact that both the range and resolution of an angle sensor, with separate PD elements, are determined by the light spot size on the focal plane of the objective lens where the PD is placed. The cell width of a multi-cell PD array should be designed to be the same or slightly smaller than the spot diameter. A PD array with 16 cells has been designed and fabricated for an angle sensor. A cell gap of 5 μm has been realized. The cell width was designed to be 40 μm based on the gap width and the spot diameter. The angle sensor has a measurement range of approximately 2300 arcsec, which is about 15 times larger than that when employing a conventional bi-cell PD. A two-dimensional PD array has also been designed and fabricated.

The third method of using single-cell photodiodes has been discussed for further improving the sensitivity for angle detection. This method can remove the influence of insensitive gaps between cells in a QPD or a bi-cell PD. The light spot focused on the photodetector can be as small as that determined by the limitation of light diffraction. This method is expected to realize a more sensitive and more compact angle sensor by using this technology.

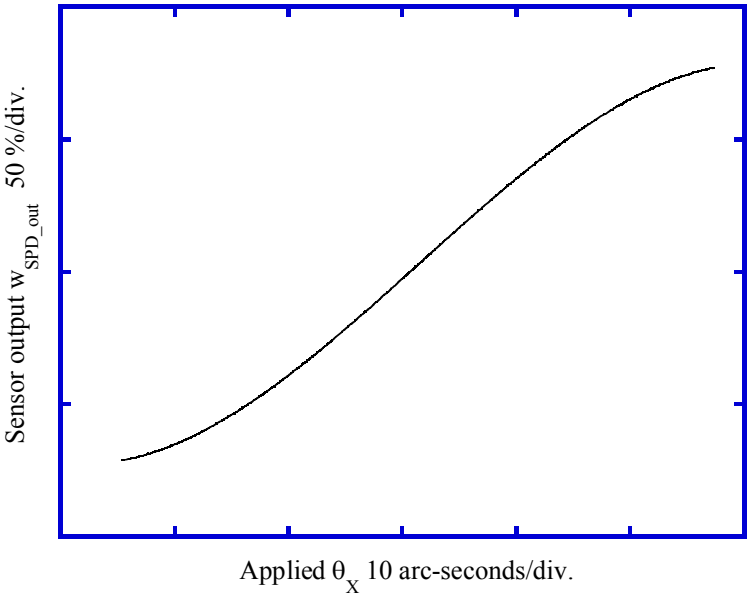

(a) θ_X

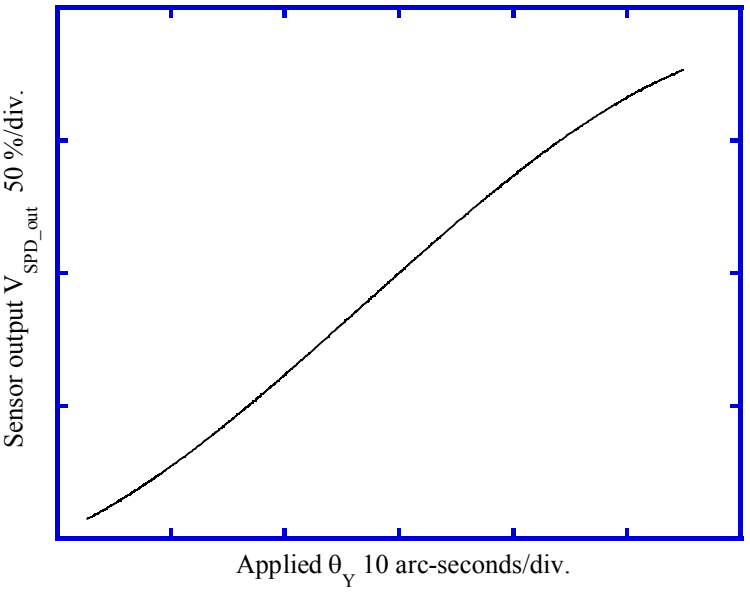

(b) θ_Y

Figure 1.31. Detection of tilt motions by the angle sensor with single-cell photodiodes

References

[1] Estler WT, Queen YH (2000) Angle metrology of dispersion prisms. Ann CIRP 49(1):415–418

[2] Farago FT, Curtis MA (1994) Handbook of dimensional measurement. Industrial Press, New York

[3] Yandayan T, Akgoz SA, Haitjema H (2002) A novel technique for calibration of polygon angles with non-integer subdivision of indexing table. Precis Eng 26(4):412–424

[4] Geckeler RD, Just A, Probst R, Weingartner I (2002) Sub-nm topography measurement using high-accuracy autocollimators. Technisches Messen 69(12):535–541

[5] Vermont Photonics Technologies Corporation (2010) http://www.vermontphotonics.com. Accessed 1 Jan 2010

[6] AMETEK Inc. (2010) http://www.taylor-hobson.com. Accessed 1 Jan 2010

[7] Jenkins FA, White HE (1976) Fundamentals of optics, chap 10. McGraw-Hill, New York

[8] Gao W, Kiyono S (1997) Development of an optical probe for profile measurement of mirror surfaces. Opt Eng 36(12):3360–3366

[9] Hamamatsu Photonics K.K. (2010) http://www.hamamatsu.com. Accessed 1 Jan 2010

[10] Bennett SJ, Gates JWC (1970) The design of detector arrays for laser alignment systems. J Phys E Sci Instrum 3:65–68

[11] OSI Systems Inc. (2010) http://www.osioptoelectronics.com. Accessed 1 Jan 2010

[12] Takacs PZ, Bresloff CJ (1996) Significant improvements in long trace profile measurement performance. SPIE Proc 2856:236–245

[13] Huang PS, Xu XR (1999) Design of an optical probe for surface profile measurement. Opt Eng 38(7):1223–1228

[14] Weingartner I, Schulz M (1999) Ultra-precise scanning technique for surface testing in the nanometric range. In: Proceedings of 9th International Conference on Precision Engineering, Osaka, Japan, pp 311–316

[15] Weingartner I, Schulz M, Elster C (1999) Novel scanning technique for ultra-precise measurement of topography. SPIE Proc 3782:306–317

[16] Gao W, Huang PS, Yamada T, Kiyono S (2002) A compact and sensitive two-dimensional angle probe for flatness measurement of large silicon wafers. Precis Eng 26(4):396–404

[17] Gao W, Ohnuma T, Satoh H, Shimizu H, Kiyono S (2004) A precision angle sensor using a multi-cell photodiode array. Ann CIRP 53(1):425–428